PHYSICAL REVIEW B **76**, 121405(R) (2007)

From graphene to graphite: A general tight-binding approach for nanoribbon carrier transport

Daniel Finkenstadt,[1,*] G. Pennington,[2] and M. J. Mehl[1]
[1]*U.S. Naval Research Laboratory, 4555 Overlook Avenue, SW, Washington DC 20375, USA*
[2]*Department of Electrical Engineering, University of Maryland, College Park, Maryland 20742, USA*
(Received 10 July 2007; revised manuscript received 24 August 2007; published 27 September 2007)

In an effort to better understand the behavior of graphene, we developed an *ab initio* parametrized fit of hydrocarbon interactions, out to arbitrary neighbors, including forces. Our computed bands show that ribbons of graphene have increased numbers of zigzag edge states, and decreased armchair band gaps, when multilayered. Armchair ribbons are known to obey three families of gap-to-width relationships; we further find that carrier group velocity v_F varies by family: small gaps have ideal v_F, and large gaps have ±20% deviations from ideal v_F. Boltzmann carrier transport simulations from calculated phonon scattering show a similar, familial conductance behavior, with peak field-effect mobility and saturated, small-field conductance increasing linearly with ribbon width.

DOI: 10.1103/PhysRevB.76.121405 PACS number(s): 73.61.Wp, 71.15.−m, 73.20.At, 73.23.−b

Recent interest in graphene has stemmed primarily from the linear band dispersion[1] near the high-symmetry vertices of its Brillouin zone, which is similar to a light Dirac fermion (DF). This analogy from relativistic quantum mechanics implies unusual properties for charge carriers in graphene, e.g., a constant carrier speed $\sim 10^6$ m/s, independent of energy,[2] a minimal conductivity, even as the number of charge carriers falls to zero,[3–5] and very low resistive losses due to scattering. This last property make graphene a useful semiconductor for device applications.[6] However, many of graphene's properties may be affected by nanoscale patterning and design. Thus, as a step toward engineering graphene devices, we study the behavior of nanographene ribbons versus edge type, width and multilayering.

For zigzag-edge nanoribbons (see Fig. 1), a metallic edge state is known to prevent a band gap from opening,[7,8] unless, as shown by recent density functional theory (DFT) results, a magnetic ordering is allowed to split edge states.[9,10] Meanwhile, armchair nanoribbons (ANRs), which orient perpendicular to the zigzag, exhibit an oscillatory gap dependence on ribbon width,[10–13] wherein every third increment of atomic row width has a different "family" of band gap, as in Fig. 2. For monolayers, tight binding does a good job of describing bands compared to DFT,[14] but since many studies treat unrelaxed, single layers with truncated neighbor interactions, they give inaccurate descriptions of edges. Also, graphene bilayers and trilayers have been studied,[15–18] but rarer are studies with more layers,[19,20] where graphene begins to approach graphite. This limit of multilayering is most interesting because massless DFs have now been observed in graphite,[21] and so it is important to characterize this transition from one layer to many.

In this paper, we study mono- and multilayer ribbons using forces, relaxations, and phonons calculated by a tight-binding Hamiltonian. To do this, we parametrized C-H interactions, out to arbitrary neighbors, via the NRL tight-binding (TB) method,[22,23] an efficient electronic-structure method using parameters fitted to DFT data. The NRL TB method gives accurate electronic structure and total energies[24] for transition metals,[25] semiconductors, and bulk graphite,[26] C_{60}, and nanotubes. Our Hamiltonian reproduced the edge states and familial band gaps, validated by DFT,[10] and we reproduced the recent, experimentally determined band structure of graphene,[20] as shown in Fig. 3(a). We find a broad class of familial dependencies that go beyond band gaps, namely, for carrier group velocity v_F, conductance G, and switching.

The Hamiltonian. To reproduce DFT accuracy, we previously fitted[27] C-C tight-binding parameters to linearized augmented plane-wave results[28,29] for diamond, graphite, and simple cubic structures and to the C_2 dimer computed with NRLMOL,[30,31] a Gaussian-based, all-electron DFT. Our parameters were fitted for a range of volumes, giving an equilibrium interatomic spacing of 1.425 Å for graphene. Within the NRL TB method, we modeled the carbon atoms using one

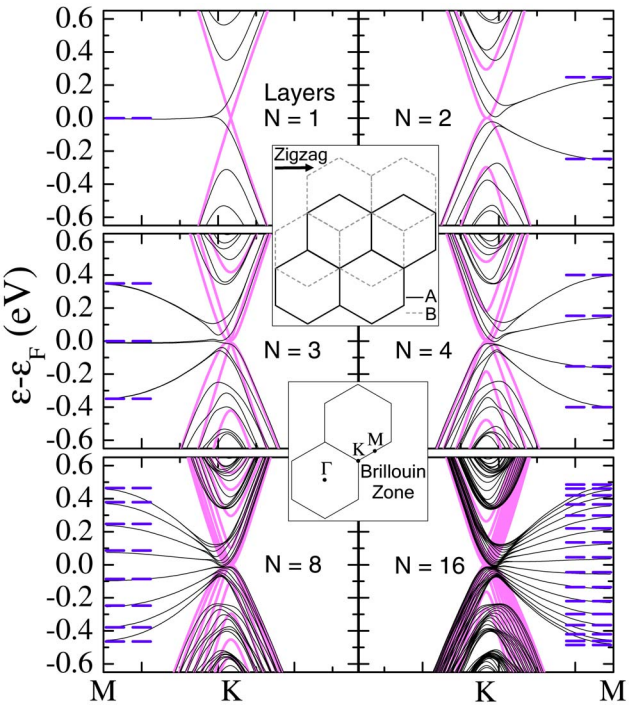

FIG. 1. (Color online) The calculated bands of 37-dimer-wide zigzag nanoribbons (black lines) and infinite sheets, shown by pink (light gray) lines. Blue (gray) double dashes are edge states with $t = 0.25$ eV in Eq. (1).

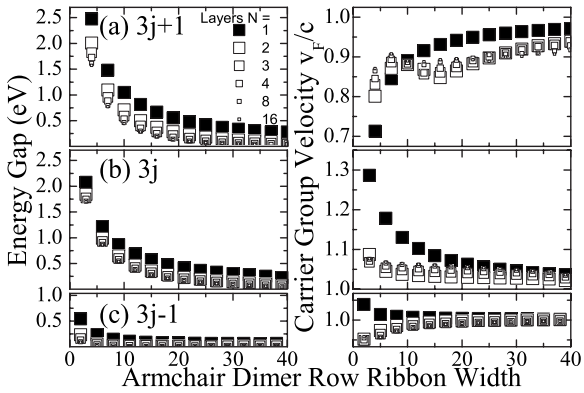

FIG. 2. Calculated band gaps of multilayer armchair nanoribbons for (a) $3j+1$, (b) $3j$, and (c) $3j-1$ increments of ribbon width (here 40 dimers=5 nm). The corresponding Fermi velocities, fitted to Eq. (2), approach $c=0.867\times10^6$ m/s.

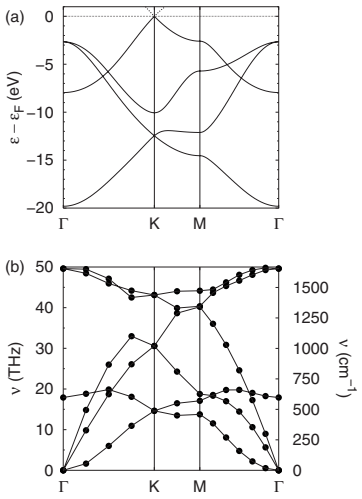

FIG. 3. Calculated graphene (a) electronic and (b) phononic band structures, with Brillouin zone labeled in Fig. 1.

s and three *p* orbitals, and hydrogen with one *s* orbital. H-H interactions were fitted to molecular levels for H_2 and a H_6 ring. The NRL TB method allows some latitude in the choice of the zeros of the total energy for individual atomic species.[22] We adjusted the energy of H_2 so that the energy difference between the bonding orbital of the H_2 molecule and the lowest 2*s* orbital of C_2 was the same as in NRLMOL. This assured no artificial charge transfer from C to H_2 at large separations. We determined the C-H interactions by freezing C-C and H-H parameters and fitted the remainder to NRLMOL data for methane, ethane, and benzene.

We tested the stability of our parameters, using molecular dynamics at 300 K, for several structures: graphene, nanotubes, nanoribbons, closed ribbons (hoops), and twisted ribbon Möbius strips. These structures were stable for times greater than 10 ps, with high-frequency vibrations, as in ideal graphene. We used a frozen-phonon approximation to study these vibrations,[22] with structures from the FROZSL symmetry code,[32] and we obtained the dispersions in Fig. 3(b), which are used in our transport simulations. For periodic ribbons, we used a linear *k*-point sampling along the reciprocal ribbon axis, including 128 points in the full Brillouin zone. For multilayers, our Hamiltonian gave a weak repulsion between layers (<150 meV/Å or 9 GPa pressure) at experimental spacings of 3.35 Å. The actual coupling of graphene is suggested to be of a van der Waals form, which is not included in our fit. We ignored this and relaxed the ionic coordinates of single graphene layers, then fixed the interlayer spacing to 3.35 Å. We also chose to focus on the Bernal *AB* stacking that shifts subsequent ribbon layers by an interatomic spacing [see Fig. 1 (inset)].

Zigzag nanoribbons. For zigzag edges, the ideal band structure of graphene is augmented by metallic edge states, shown in Fig. 1. These states are numerous in multilayers but may be fitted to a molecular-chain spectrum,

$$\varepsilon_n = 2t\cos[m\pi/(N+1)], \tag{1}$$

with hopping energy $t=0.25$ eV, layers N, and $m=1,\ldots,N$. There is a spin degeneracy for these levels, for which DFT gives a 0.3 eV splitting, for narrow ribbons.[10] Odd multilayers are special with regard to this splitting, exhibiting massless DFs in sheets (X bands in Fig. 1; $N=1,3$) and an ε_F-centered edge state in ribbons. While the odd-*N* edge state is split by magnetic ordering, opening a gap, the even-*N* edge states in Eq. (1) lie above and below ε_F, so splitting would *close* a gap. In the graphtitic $N\to\infty$ limit, these bands collapse into mostly parabolic bundles, but, for *N* odd, graphite still allows coexisting massless and massive DFs.[21]

Notably, it has been shown that even a partial component of zigzag edge will introduce states at ε_F.[8] This is crucial for comparison to experiment,[33] as most random edge shapes will have metallic states.[34,35] For most ribbons more than 5 nm wide, we thus expect very small gaps.

Armchair nanoribbons. The armchair nanoribbon exhibits hyperbolic bands that approach the ideal form

$$\varepsilon_k = \pm\sqrt{(\varepsilon_{gap}/2)^2+(\hbar v_F k)^2}, \tag{2}$$

which is the energy dispersion of a relativistic particle with momentum $\hbar k$, effective "mass" $\varepsilon_{gap}/2v_F^2$, and "speed of light" v_F. In Fig. 2, we plot the parameters for a relaxed monolayer (filled symbols). The plots are separated by family, as in Ref. 10, one width increment per panel. The $3j-1$ family is metallic in first-nearest-neighbor tight binding, but a gap opens when edge atoms vary in coupling strength or by including third neighbors.[14,36] These corrections to simple tight-binding theory explain why a gap opens; in this case we include all neighbors, with forces, to relax structures.

For multilayers that approach graphite, we found that ε_{gap} was reduced from the monolayer case. The largest reduction in ε_{gap} is a decrease of 0.2–0.5 eV going from monolayers to bilayers, while the change in going to trilayers is less than 0.2 eV. The 8–16 layers are converged with differences of below 10 meV. We thus expect that a 2–8 layered ANR will have a nearly graphitic band gap of less than 80 meV for widths greater than 5 nm, and for transistor applications, this favors narrow monolayer ribbons. As transistors based on graphene may require an ε_{gap} of ~0.25 eV,[6] the monolayer is still the best candidate for a transistor device.

Armchair nanoribbon transport. Understanding and pre-

dicting carrier transport and scattering in graphite nanoscale ribbons (GNRs) is important for potential nanoscale device applications, including use as ultrasmall transistors and as (bio)/chemical sensors. Semiconducting GNRs, including ANRs, are best suited for such applications since a gate potential may effectively turn the device current on and off by moving the Fermi level into and out of the carrier bands.

Previous transport studies have focused mainly on the ballistic transport regime.[37] Here we focus on phonon-limited semiclassical transport, a regime that has been shown to describe many transport features in carbon nanotubes,[38] but has received only limited attention in nanoribbons.[6] Semiclassical transport is applicable when the carrier mean free path between scattering events is much larger than the ribbon length L. This transport regime is of interest since (1) it allows for the incorporation of a relatively simple and highly predictive scattering theory,[39] (2) many of the bulk transport features obtained are also found in other regimes, and (3) it gives the limits of the ballistic and phase-coherent transport regimes. Phonon scattering will be considered since this mechanism is found to be significant in similar materials such as graphite[40] and carbon nanotubes.[38] As both transport and associated scattering mechanisms depend strongly on the low-energy electronic structure of carriers, we find that important semiclassical transport properties also vary with the three ANR families.

Semiclassical carrier transport is studied by solving a one-dimensional, steady-state, Boltzmann transport equation,

$$\frac{eF}{\hbar}\frac{\partial f_k}{\partial k} = \sum_q [f_{k+q}(1-f_k)S_{k+q,k} - f_k(1-f_{k+q})S_{k,k+q}],$$

for the nonequilibrium carrier distribution function f_k, in a small externally applied axial field F ($<k_BT/L$), and using the carrier-phonon scattering rate $S_{k,k+q}$ for axial momentum transfer $k \rightarrow k+q$ (wave vectors take on ± values). Only the first electron subband is considered. Along with the scattering rate, f_k will be determined by the density of occupied carriers n. If the band structure is known, n can be found from the Fermi level, which is set by the application of the transistor gate voltage. Using first-order perturbation theory, the scattering rate is

$$S_{k,k+q} = \frac{\hbar D^2(q)\mathcal{D}(k+q)}{\pi\rho E_{ph} w}\left(N_{ph}(E_{ph}) + \frac{1}{2} \pm \frac{1}{2}\right),$$

with $D=16\ \mathrm{eV}\times q$ the in-plane acoustic deformation potential of graphite,[40] $\rho=7.6\times10^{-7}\ \mathrm{kg/m^2}$ for graphene, ribbon width w, and Bose-Einstein phonon occupation N_{ph} (at 300 K). The ± is for emission and absorption. The carrier density of states ($\mathcal{D}$) is given by $2[1+(\varepsilon_{gap}/2\hbar v_F k)^2]^{1/2}/\hbar v_F$, where v_F and ε_{gap} vary by family. The phonon energy E_{ph} is taken from the frozen phonon results along Γ-M in Fig. 3(b). The graphene phonon spectrum is used here since only one subband is considered. In this case, the relevant phonons that mediate intrasubband scattering are insensitive to ribbon edge effects. Lastly, since we focus on long, thin ribbons, we consider only longitudinally polarized phonons.

Once f_k is found, the conductance is given by[38]

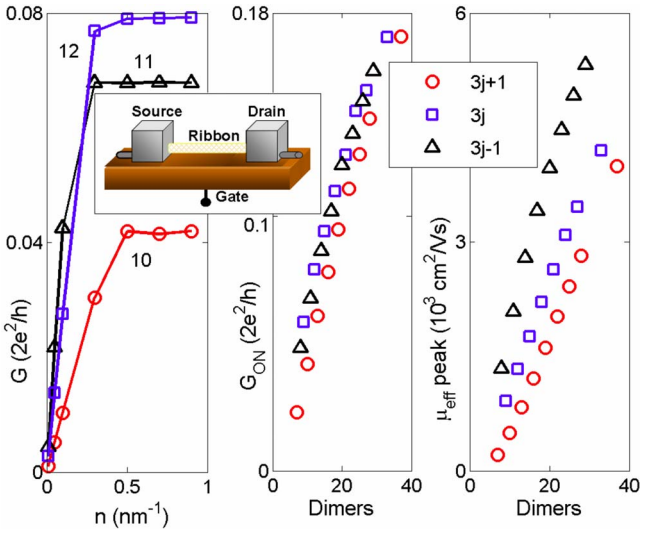

FIG. 4. (Color online) Small-field approximated conductance of an armchair nanoribbon transistor (inset) showing variations among the three families: ○, □, △. Colors and lines guide the eye. Panels (left to right) show conductance versus carrier density, maximum (on) (i.e., saturated) conductance versus dimer row number, and peak field-effect mobility.

$$G = 2\frac{env_F}{FL}\sum_k \mathrm{sgn}(k) f_k\left(1 + \frac{\varepsilon_{gap}^2}{4\hbar^2 v_F^2 k^2}\right) \Big/ \sum_k f_k,$$

with the slope of G giving the field-effect mobility μ_{eff} as $(L/e)\partial G/\partial n$. Transport simulations of an ANR transistor device are shown in Fig. 4, where G is found to exhibit well-defined "on" and "off" states as n is varied. The on-state conductance G_{on} is reached as $n(\varepsilon_F)$ approaches the minimum value of $2/\hbar v_F$, and G_{on} increases with v_F as a result of fast moving carriers and a smaller $\mathcal{D}$ for backscattering. The turn-on characteristics of the ANRs are represented by the peak field-effect mobility μ_{eff} which occurs when n is small. Larger peak values occur as ε_{gap} decreases and as v_F increases. The on-state conductance and the peak mobility are both found to increase roughly linearly as a function of ribbon width (dimer rows). The former result agrees with recent experimental measurements of G_{on}.[33] Expected trends are found when the transport properties of the ANR are compared; the $3j-1$ and $3j$ families have the largest μ_{eff}; the $3j$ family has larger G_{on} since v_F is larger. Multilayer ANRs will turn on at lower applied gate voltages due to decreased band gaps, and G will be lowered for two reasons: (1) layering increases $\mathcal{D}$ to scatter into, and (2) lower v_F increases the $\mathcal{D}$ in valence and conduction bands. Transport in the edge states of zigzag ribbons would require a distinct theoretical treatment as these states are expected to interact relatively strongly with the ribbon edge. Transport in such states would likely depend on the nature of edge phonons and the roughness of the ribbon edge. The conducting states of ANRs do not overlap as significantly with the ribbon edge and therefore would experience a reduction in edge scattering when compared to the zigzag edge states. Our results also show that characteristic band structure variations among the ANR

families should lead to variations in carrier transport, e.g., in transistors or in sensor applications that exploit the sensitive edge-bonding characteristics.

Conclusions. By developing a fully general tight-binding Hamiltonian from first principles, we were able to study graphene with arbitrary neighbor interactions, hydrogen termination, and layering. We found that layered ribbons of graphene approach the familiar band structure of graphite with increasing ribbon width, except for zigzag edge states near the Fermi level. These states do not occur for armchair edges, which instead have a finite energy gap over a range of layer and width families. Only for monolayers less than 5 nm wide do we find an appreciable band gap for engineering devices as proposed by Obradovic *et al.*[6] Accordingly, we simulated nanoribbon transistors, in a phonon-scattering-limited regime. Extensions of the three-family band-gap behavior[10] were found for carrier group velocity, conductance, and field-effect mobility. Interestingly, two families of ribbons had large gaps but opposite deviations in ideal carrier group velocity with respect to the strip width. These deviations gave slow and fast switching characteristics, since a gate voltage can turn the nanoribbon transistor on (saturated) or off. Such devices could be exploited for nanoscale electronics and also for chemical sensing based on the sensitivity of nanoribbons to edge states.

We acknowledge the support of the Office of Naval Research, DOD HPCMPO CHSSI, and the National Research Council. We thank M. S. Fuhrer for fruitful discussions and C. Ashman at HPTI for code support.

*daniel.kris@gmail.com

[1] P. R. Wallace, Phys. Rev. **71**, 622 (1947).
[2] K. S. Novoselov, A. K. Geim, S. V. Morozov, D. Jiang, M. I. Katsnelson, I. V. Grigorieva, S. V. Dubonos, and A. A. Firsov, Nature (London) **438**, 197 (2005).
[3] E. Fradkin, Phys. Rev. B **33**, 3263 (1986).
[4] M. I. Katsnelson, Eur. Phys. J. B **51**, 157 (2006).
[5] J. Tworzydlo, B. Trauzettel, M. Titov, A. Rycerz, and C. W. J. Beenakker, Phys. Rev. Lett. **96**, 246802 (2006).
[6] B. Obradovic, R. Kotlyar, F. Heinz, P. Matagne, T. Rakshit, M. D. Giles, M. A. Stettler, and D. E. Nikonov, Appl. Phys. Lett. **88**, 142102 (2006).
[7] M. Fujita, K. Wakabayashi, K. Nakada, and K. Kusakabe, J. Phys. Soc. Jpn. **65**, 1920 (1996).
[8] K. Nakada, M. Fujita, G. Dresselhaus, and M. S. Dresselhaus, Phys. Rev. B **54**, 17954 (1996).
[9] H. Lee, Y.-W. Son, N. Park, S. Han, and J. Yu, Phys. Rev. B **72**, 174431 (2005).
[10] Y.-W. Son, M. L. Cohen, and S. G. Louie, Nature (London) **444**, 347 (2006); Phys. Rev. Lett. **97**, 216803 (2006).
[11] M. Ezawa, Phys. Rev. B **73**, 045432 (2006).
[12] L. Brey and H. A. Fertig, Phys. Rev. B **73**, 235411 (2006).
[13] H. Zheng, Z. F. Wang, T. Luo, Q. W. Shi, and J. Chen, Phys. Rev. B **75**, 165414 (2007).
[14] S. Reich, J. Maultzsch, C. Thomsen, and P. Ordejon, Phys. Rev. B **66**, 035412 (2002).
[15] P. E. Lammert, P. Zhang, and V. H. Crespi, Phys. Rev. Lett. **84**, 2453 (2000).
[16] J. Nilsson, A. H. Castro Neto, N. M. R. Peres, and F. Guinea, Phys. Rev. B **73**, 214418 (2006).
[17] F. Guinea, A. H. Castro Neto, and N. M. R. Peres, Phys. Rev. B **73**, 245426 (2006).
[18] S. Latil and L. Henrard, Phys. Rev. Lett. **97**, 036803 (2006).
[19] J. L. Manes, F. Guinea, and M. A. H. Vozmediano, Phys. Rev. B **75**, 155424 (2007).
[20] T. Ohta, A. Bostwick, J. L. McChesney, T. Seyller, K. Horn, and E. Rotenberg, Phys. Rev. Lett. **98**, 206802 (2007).
[21] G. Li and E. Y. Andrei, Nat. Phys. **3**, 623 (2007).
[22] R. E. Cohen, M. J. Mehl, and D. A. Papaconstantopoulos, Phys. Rev. B **50**, 14694 (1994); M. J. Mehl and D. A. Papaconstantopoulos, *ibid.* **54**, 4519 (1996).
[23] D. A. Papaconstantopoulos and M. J. Mehl, J. Phys.: Condens. Matter **15**, R413 (2003), and references therein.
[24] C. M. Goringe, D. R. Bowler, and E. Hernandez, Rep. Prog. Phys. **60**, 1447 (1997).
[25] D. Finkenstadt, N. Bernstein, J. L. Feldman, M. J. Mehl, and D. A. Papaconstantopoulos, Phys. Rev. B **74**, 184118 (2006).
[26] D. A. Papaconstantopoulos, M. J. Mehl, S. C. Erwin, and M. R. Pederson, in *Tight-Binding Approach to Computational Materials Science*, edited by P. Turchi, A. Gonis, and L. Colombo, MRS Symposia Proceedings No. 491 (Materials Research Society, Pittsburgh, 1998), p. 221.
[27] The parameters used in this paper are available from the authors, or at http://cst-www.nrl.navy.mil/bind/
[28] O. K. Andersen, Phys. Rev. B **12**, 3060 (1975).
[29] D. Singh, H. Krakauer, and C. S. Wang, Phys. Rev. B **34**, 8391 (1986).
[30] M. R. Pederson and K. A. Jackson, Phys. Rev. B **41**, 7453 (1990); K. A. Jackson and M. R. Pederson, *ibid.* **42**, 3276 (1990).
[31] M. R. Pederson, D. V. Porezag, J. Kortus, and D. C. Patton, Phys. Status Solidi B **217**, 197 (2000).
[32] H. T. Stokes and L. L. Boyer, Computer code, FROZSL, http://www.physics.byu.edu/~stokesh/isotropy.html
[33] M. Y. Han, B. Ozyilmaz, Y. Zhang, and P. Kim, Phys. Rev. Lett. **98**, 206805 (2007).
[34] Y. Kobayashi, K. I. Fukui, T. Enoki, K. Kusakabe, and Y. Kaburagi, Phys. Rev. B **71**, 193406 (2005).
[35] Y. Kobayashi, K. I. Fukui, T. Enoki, and K. Kusakabe, Phys. Rev. B **73**, 125415 (2006).
[36] C. T. White, J. Li, D. Gunlucke, and J. W. Mintmire, Nano Lett. **7**, 825 (2007).
[37] D. A. Areshkin, D. Gunlycke, and C. T. White, Nano Lett. **7**, 204 (2007); D. Gunlycke, H. M. Lawler, and C. T. White, Phys. Rev. B **75**, 085418 (2007).
[38] G. Pennington and N. Goldsman, Phys. Rev. B **68**, 045426 (2003); G. Pennington, N. Goldsman, A. Akturk, and A. E. Wickenden, Appl. Phys. Lett. **90**, 062110 (2007).
[39] M. Lundstrom, *Fundamentals of Carrier Transport*, 2nd ed. (Cambridge University Press, Cambridge, U.K., 2000).
[40] K. Sugihara, Phys. Rev. B **28**, 2157 (1983).